Fluoro-apatite and Calcium Phosphate Nanoparticles by Flame Synthesis

Stefan Loher,[†,‡] Wendelin J. Stark,*[,†,‡] Marek Maciejewski,[†] Alfons Baiker,[†] Sotiris E. Pratsinis,[‡] Dennis Reichardt,[§] Fabrice Maspero,[§] Frank Krumeich,[||] and Detlef Günther[||]

Institute for Chemical and Bioengineering, Department of Chemistry and Applied Biosciences, ETH Hoenggerberg, CH-8093 Zurich, Switzerland, Particle Technology Laboratory, Department of Mechanical and Process Engineering, ETH Zentrum, CH-8092 Zurich, Switzerland, Degradable Solutions AG, CH-8952 Schlieren, Switzerland, and Laboratory of Inorganic Chemistry, Department of Chemistry and Applied Biosciences, ETH Hoenggerberg, CH-8093 Zurich, Switzerland

Received July 27, 2004. Revised Manuscript Received October 8, 2004

Calcium phosphate nanoparticles with calcium/phosphorus molar ratios ranging from 1.43 to 1.67 have been synthesized by simultaneous combustion of calcium carboxylate and tributyl-phosphate based precursors in a flame spray reactor. Fluoro-apatite and zinc or magnesium doped calcium phosphates were obtained by adding trifluoroacetic acid or corresponding carboxylates into the fuel. Nanoparticle morphology and the structure of sintered ceramics were studied using transmission and scanning electron microscopy. Thermal evolution of calcium phosphate phases was investigated by powder X-ray diffraction, Fourier transform infrared spectroscopy, and thermal analysis. A molar ratio of Ca/P < 1.5 in the precursor promoted the formation of dicalcium pyrophosphate ($Ca_2P_2O_7$). Phase pure β-tricalcium phosphate was obtained with a precursor Ca/P ratio of 1.52 after subsequent calcination at 900 °C. The regular, open structure with interconnecting micropores and the facile substitution of both anions and cations suggests possible application as a biomaterial.

Introduction

Calcium phosphate biomaterials have attracted tremendous interest in clinical medicine. Both hydroxyapatite (HAp, $Ca_{10}(PO_4)_6(OH)_2$) and tricalcium phosphate (TCP, $Ca_3(PO_4)_2$) exhibit excellent biocompatibility and osteoconductivity.[1−3] They are widely used for repair of bony or periodontal defects, coating of metallic implants, and bone space fillers. Traditional methods (precipitation, sol−gel synthesis, hydrothermal method, or solid-state reactions)[1,4−6] give access to a limited range of compositions with specific morphology. Pure β-tricalcium phosphate is traditionally prepared either by solid-state reaction[7] or by sintering calcium-deficient apatite ($Ca_9(HPO_4)(PO_4)_5(OH) \rightarrow 3Ca_3(PO_4)_2 + H_2O$) obtained by precipitation.[8] Liquid preparations require careful control of synthesis parameters (pH and temperature) following time- and cost-intensive after-treatments such as washing, drying, and calcination.

Solid-state reactions involve thorough mixing of precursor powders followed by prolonged sintering and mostly result in low specific surface area powders. Once implanted, these rather dense materials can display a lack of microporosity with reduced contact to the body fluid hindering resorption in vivo. The sol−gel synthesis[9] offers a production method for very homogeneous materials which is attributed to the intimate mixing of calcium and phosphorus precursors. Unfortunately, reproducible preparation is restricted to hydroxyapatite. With growing demands for more complex morphology or compositions, alternative preparation methods such as plasma spraying[10,11] and pulsed laser deposition[12] have resulted in advantageous coatings on implant surfaces. Amorphous calcium phosphates have shown to result in improved resorption properties[13,14] and offer valuable materials for self-setting cements.[15] Beyond mere bioactivity and resorption properties, bioceramics which allow stimulation of cellular responses at the molecular level are in high demand.[16] Such tailored third-generation biomaterials contain

* To whom correspondence should be addressed. E-mail: wendelin.stark@chem.ethz.ch.
† Institute for Chemical and Bioengineering, ETH Hoenggerberg.
‡ Particle Technology Laboratory, ETH Zentrum.
§ Degradable Solutions AG.
|| Laboratory of Inorganic Chemistry, ETH Hoenggerberg.

(1) Jarcho, M. *Clin. Orthop. Relat. Res.* **1981**, 259−278.
(2) de Groot, K. *Bioceramics of Calcium Phosphate*; CRC Press: Boca Raton, FL, 1983.
(3) Hanker, J. S.; Giammara, B. L. *Science* **1988**, *242*, 885−892.
(4) LeGeros, R. Z. *Calcium Phosphates in Oral Biology and Medicine*; S. Karger: Basel, 1991; Vol. 15.
(5) Metsger, D. S.; Driskell, T. D.; Paulsrud, J. R. *J. Am. Dent. Assoc.* **1982**, *105*, 1035−1038.
(6) LeGeros, R. Z.; LeGeros, J. P.; Daculsi, G.; Kijkowska, R. *Encyclopedic Handbook of Biomaterials and Bioengineering*; Marcel Dekker: New York, 1995; Vol. Part A.
(7) Yang, X. H.; Wang, Z. H. *J. Mater. Chem.* **1998**, *8*, 2233−2237.
(8) Bouler, J. M.; LeGeros, R. Z.; Daculsi, G. *J. Biomed. Mater. Res.* **2000**, *51*, 680−684.
(9) Jillavenkatesa, A.; Condrate, R. A. *J. Mater. Sci.* **1998**, *33*, 4111−4119.
(10) Maxian, S. H.; Zawadsky, J. P.; Dunn, M. G. *J. Biomed. Mater. Res.* **1993**, *27*, 717−728.
(11) Dong, Z. L.; Khor, K. A.; Quek, C. H.; White, T. J.; Cheang, P. *Biomaterials* **2003**, *24*, 97−105.
(12) Arias, J. L.; Mayor, M. B.; Pou, J.; Leng, Y.; Leon, B.; Perez-Amor, M. *Biomaterials* **2003**, *24*, 3403−3408.
(13) Sarkar, M. R.; Wachter, N.; Patka, P.; Kinzl, L. *J. Biomed. Mater. Res.* **2001**, *58*, 329−334.
(14) Overgaard, S.; Bromose, U.; Lind, M.; Bunger, C.; Soballe, K. *J. Bone Jt. Surg., Br. Vol.* **1999**, *81B*, 725−731.

10.1021/cm048776c CCC: $30.25
Published on Web 12/01/2004

additional ions which have been suggested for their bone-growth inducing properties.

Flame spray pyrolysis[17] has established itself as a suitable method for the preparation of nanoparticles, most notably, oxides containing main group and transition metals.[18−21] It has rapidly evolved into a scalable process for oxide nanoparticles for possible applications in various fields.[22] The industrial-scale flame-aerosol synthesis today produces megaton quantities of carbon, silica, and titania nanoparticles.

In the present study, we would like to extend the range of accessible flame-made nanoparticles from metals or oxides to metal salts. The method is illustrated for the preparation of calcium phosphates and results in α-, *β*-, or amorphous tricalcium phosphate, calcium pyrophosphate, and hydroxy- or fluoro-apatite. Cation doping is illustrated by incorporation of biologically important magnesium or zinc ions.

Experimental Section

Materials Preparation. Calcium phosphate was prepared by flame spray pyrolysis[17] using calcium oxide (99.9%, Aldrich) dissolved in 2-ethylhexanoic acid (purum., ≥98%, Fluka) and tributyl phosphate (puriss., ≥99%, Fluka) as precursors.[23,24] The calcium content of the Ca-precursor was determined by complexometry with ethylenediaminetetraacetic acid disodium salt dihydrate (≥ 99%, Fluka) to be 0.768 mol/kg. Starting from a parent solution (38 mL per run) with a calcium to phosphorus molar ratio (Ca/P) of 1.5, the various mixtures ranging from 1.43 ≤ Ca/P ≤ 1.67 have been obtained by adding corresponding amounts of either calcium 2-ethylhexanoate or tributyl phosphate. For the half- ($Ca_{10}(PO_4)_6$-(OH)F) and fully- ($Ca_{10}(PO_4)_6F_2$) fluoro-substituted hydroxyapatites, trifluoroacetic acid (99%, Riedel deHaen) has been correspondingly mixed with precursors having a molar ratio of Ca/P = 1.67 (apatite stoichiometry). Magnesium or zinc containing tricalcium phosphate (nominal content 0.24 wt % Mg or 0.41 wt % Zn) and hydroxyapatite (0.29 wt % Mg or 0.51 wt % Zn) have been prepared by admixing corresponding amounts of magnesium oxide (≥98%, Fluka) dissolved in 2-ethylhexanoic acid or zinc naphthenate (≤50% in mineral spirits, Aldrich) to the precursor. Throughout all the experiments, the concentration of the precursor solutions was kept constant (0.667 mol/L) by adding xylene (96%, Riedel deHaen).

The liquid mixtures were fed through a capillary (diameter 0.4 mm) into a methane/oxygen flame at a rate of 5 mL/min. Oxygen (5 L/min, 99.8%, Pan Gas) was used to disperse the liquid leaving the capillary. The pressure drop at the capillary tip (1.5 bar) was kept constant by adjusting the orifice gap area at the nozzle. A stable combustion was achieved by applying a sheath gas (oxygen, 230 L/h, 99.8%, Pan Gas) through a concentric sinter metal ring. Calibrated mass flow controllers (Bronkhorst) were used to monitor all gas flows. The as-formed particles were collected on a glass fiber filter (Whatmann GF/A, 25.7-cm diameter), placed on a cylinder mounted above the flame, by the aid of a vacuum pump (Vaccubrand). Thermal treatment (30 min at specified temperature) was conducted in a preheated laboratory furnace (Thermolyne Type 48000) followed by quenching in air at ambient conditions.

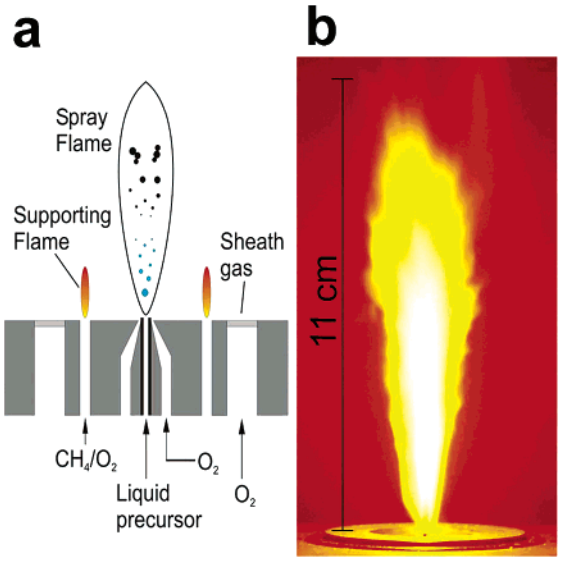

Figure 1. (a) Sketch of the experimental setup for the preparation of flame-made nanoparticles.[17] The precursor mixture is dispersed by oxygen (center) and fed into the methane/oxygen supporting flame. (b) The burning spray of a calcium phosphate producing flame synthesis unit shows the typical orange emission light of calcium. Nanoparticles leave the flame at the top where they are collected on a filter.

Characterization. The specific surface area of the powders was measured on a Tristar (Micromeritics Instruments) instrument by nitrogen adsorption at 77 K using the Brunauer−Emmett−Teller (BET) method. All samples were outgassed at 150 °C for 1 h. Thermal effects were detected by means of differential scanning calorimetry (DSC) on a Netzsch STA 409 simultaneous thermal analyzer connected to a mass spectrometer (Balzers QMG 420). X-ray powder diffraction (XRD) patterns were collected on a Bruker D 8 Advance diffractometer from 20° to 40° at a step size of 0.12° and a scan speed of 2.4°/min at ambient condition. For Fourier transform infrared (FTIR) spectroscopy, pellets of 200 mg of KBr (≥99.5%, Fluka) and 0.5 mg of sample were prepared and dehydrated in a drying furnace at 80 °C/<10 mbar for at least 8 h before examination (4000 $cm^{-1} < \lambda < 400\ cm^{-1}$) on a Perkin-Elmer Spectrum BX (4 scans) with 4 cm^{-1} resolution. Elemental analysis was performed by laser ablation inductively coupled plasma mass spectrometry (LA-ICP-MS).[25] Samples were pressed into plates and irradiated with an excimer laser (Lambda Physik Compex 110 I; ArF, 193 nm, pulse energy 150 mJ, frequency 10 Hz). The vaporized material was carried by a helium stream to an ICP mass spectrometer (Perkin-Elmer Elan 6100) and analyzed for calcium (^{42}Ca, ^{43}Ca, ^{44}Ca), phosphorus (^{31}P), magnesium (^{24}Mg, ^{25}Mg, ^{26}Mg), and zinc (^{64}Zn, ^{66}Zn, ^{67}Zn). External calibration was carried out using the Reference 610 from NIST and a fluoroapatite (Durango). In all cases the Ca signal was used as an internal standard quantification. The transmission electron microscopy (TEM) pictures were recorded on a CM30 ST (Philips, LaB_6 cathode, operated at 300 kV, point resolution ~2 Å). Particles were

(15) Knaack, D.; Goad, M. E. P.; Aiolova, M.; Rey, C.; Tofighi, A.; Chakravarthy, P.; Lee, D. D. *J. Biomed. Mater. Res.* **1998**, *43*, 399−409.
(16) Hench, L. L.; Polak, J. M. *Science* **2002**, *295*, 1014−1017.
(17) Madler, L.; Kammler, H. K.; Mueller, R.; Pratsinis, S. E. *J. Aerosol. Sci.* **2002**, *33*, 369−389.
(18) Stark, W. J.; Kammler, H. K.; Strobel, R.; Gunther, D.; Baiker, A.; Pratsinis, S. E. *Ind. Eng. Chem. Res.* **2002**, *41*, 4921−4927.
(19) Strobel, R.; Stark, W. J.; Madler, L.; Pratsinis, S. E.; Baiker, A. *J. Catal.* **2003**, *213*, 296−304.
(20) Kim, S.; Gislason, J. J.; Morton, R. W.; Pan, X. Q.; Sun, H. P.; Laine, R. M. *Chem. Mater.* **2004**, *16*, 2336−2343.
(21) Marchal, J.; John, T.; Baranwal, R.; Hinklin, T.; Laine, R. M. *Chem. Mater.* **2004**, *16*, 822−831.
(22) Stark, W. J.; Pratsinis, S. E. *Powder Technol.* **2002**, *126*, 103−108.
(23) Stark, W. J.; Mädler, L.; Pratsinis, S. E. International patent application WO 2004/005184, pending, 2004.
(24) Loher, S.; Maciejewski, M.; Pratsinis, S. E.; Baiker, A.; Stark, W. J.: International patent application, pending, 2004.
(25) Gunther, D.; Frischknecht, R.; Heinrich, C. A.; Kahlert, H. J. *J. Anal. At. Spectrom.* **1997**, *12*, 939−944.

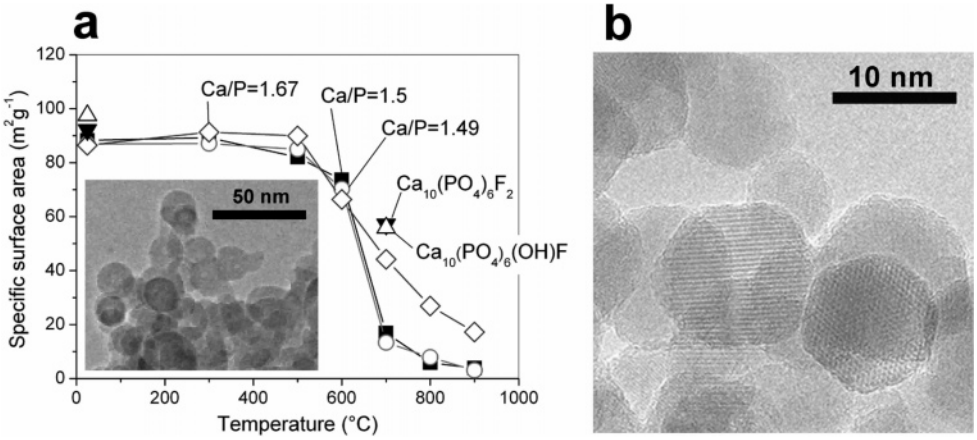

Figure 2. (a) Dependence of BET surface area on calcination temperature (duration 30 min in air) of different calcium phosphate materials and fluoride-substituted hydroxyapatite. Sintering is indicated by a pronounced drop at 600 °C showing the onset of crystallization. Inset: Transmission electron microscopy image of as-prepared nanoparticles. (b) A transmission electron microscopy image of fluoride-substituted hydroxyapatite ($Ca_{10}(PO_4)_6(OH)F$) after synthesis shows distinct crystal planes and regular particles.

Table 1. Ca/P Ratio of As-Prepared Samples

sample	Ca/P ratio (nominal)	Ca/P ratio[a] (measured)
Ca/P = 1.5	1.500	1.50
Ca/P = 1.52	1.515	1.52
Ca/P = 1.67	1.667	1.64

[a] Error: ±0.02.

deposited onto a carbon foil supported on a copper grid. Scanning electron microscopy (SEM) investigations were performed with a Leo 1530 Gemini (Zeiss) operated at 1 kV.

Results and Discussion

Calcium phosphate nanoparticles of various Ca/P molar ratios were prepared by flame spray pyrolysis. Experimentally, the flame spray reactor (Figure 1a) consists of a capillary surrounded by a narrow, adjustable orifice. The precursor liquid is dispersed at the tip resulting in a well-defined spray. A surrounding methane/oxygen supporting flame ignites the spray (Figure 1b) and the flame converts the precursor mixture to the corresponding materials. Spherical, highly agglomerated particles of 10−30-nm diameter (inset in Figure 2a) were collected after synthesis. Elemental analysis confirmed that the composition of the precursor mixture was preserved in the product powder (Table 1).

Textural properties, thermal stability, and evolution of different crystal phases were followed by nitrogen adsorption (BET), X-ray diffraction (XRD), and differential scanning calorimetry (DSC) coupled with mass spectrometry (MS). As-prepared nanoparticles typically exhibit about 90 m^2/g (BET equivalent diameter 20 nm). Calcination results in a steep decrease of specific surface area around 600 °C indicating the onset of strong sintering and crystallization (Figure 2a). While a slight excess of phosphorus (Ca/P = 1.49) had no significant influence on the thermal stability, hydroxyapatite (Ca/P = 1.67) is considerably more stable and maintains a surface area above 15 m^2/g at 900 °C.

The histological behavior of biomaterials in vivo is strongly determined by morphology and phase composition. Macropores (diameter >100 μm) provide a scaffold for bone-cell colonization and therefore favor bone ingrowth.[26,27] The content of micropores (diameter < 10 μm) is given by the preparation method and the sintering temperature and duration. Interconnective microporosity guarantees body fluid circulation and is even believed to be responsible for the observed osteoinductive properties of certain bioceramics.[28,29] Electron microscopy images of Ca/P = 1.5 nanoparticles after calcination at 700 °C (Figure 3a and b) reveal that the material has fused together, building clearly visible sinter necks. It preserves a high porosity with a primary particle size of about 100 nm. Sintering at 900 °C (Figure 3c and d) results in much larger primary particles of approximately 0.5-μm diameter. The highly regular structure with interconnecting micropores is favorable for resorption properties and the induction of bone formation in vivo.

As-prepared calcium phosphate consists of amorphous nanoparticles indicating that the fast cooling after the formation in the flame did not allow the material to crystallize. The presence of a glassy, amorphous structure was confirmed by XRD and thermal analysis. Coupled with mass spectrometry (TA-MS), it allowed simultaneous detection of desorbing water and carbon dioxide (Figure 4). Combining DSC curves and XRD patterns (Figure 5a and b) provides information about crystallization and phase transformations. The exothermic peak around 600 °C correlates to the crystallization of the amorphous material. The sample Ca/P = 1.52 (Ca/P = 1.5 + 1 at. % Ca), amorphous at 500 °C (Figure 5, trace 1), crystallizes to meta-stable α-TCP,[30] often referred to as α'-TCP (Figure 5, trace 2). Above 850 °C α'-TCP transforms into the thermodynamically favored β-TCP (Figure 5, trace 3), which is stable up to 1150 °C, where it transforms endothermically back into the high-temperature polymorph α-TCP. Changing the stoichiometry toward lower Ca/P ratios provokes the formation of pyrophosphate $Ca_2P_2O_7$. Crystallization of α-dicalcium

(26) Gauthier, O.; Bouler, J. M.; Aguado, E.; Pilet, P.; Daculsi, G. *Biomaterials* **1998**, *19*, 133−139.
(27) Weiss, P.; Obadia, L.; Magne, D.; Bourges, X.; Rau, C.; Weitkamp, T.; Khairoun, I.; Bouler, J. M.; Chappard, D.; Gauthier, O.; Daculsi, G. *Biomaterials* **2003**, *24*, 4591−4601.
(28) Bignon, A.; Chouteau, J.; Chevalier, J.; Fantozzi, G.; Carret, J. P.; Chavassieux, P.; Boivin, G.; Melin, M.; Hartmann, D. *J. Mater. Sci.: Mater. Med.* **2003**, *14*, 1089−1097.
(29) Yuan, H. P.; de Bruijn, J. D.; Li, Y. B.; Feng, J. Q.; Yang, Z. J.; de Groot, K.; Zhang, X. D. *J. Mater. Sci.: Mater. Med.* **2001**, *12*, 7−13.
(30) Somrani, S.; Rey, C.; Jemal, M. *J. Mater. Chem.* **2003**, *13*, 888−892.

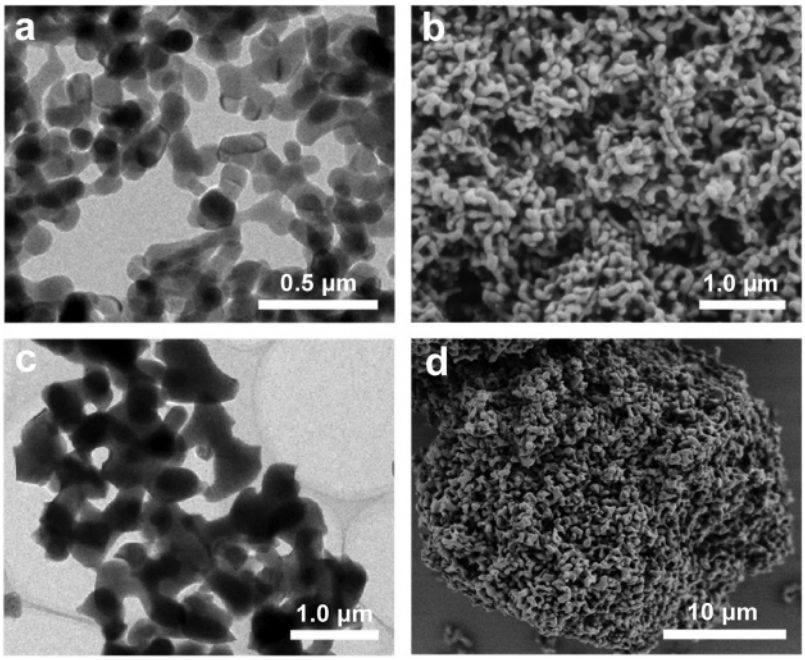

Figure 3. Transmission electron microscopy (left) and scanning electron microscopy (right) images of calcium phosphate. Metastable α-tricalcium phosphate resulting from calcination (30 min) at 700 °C (a and b). *β*-tricalcium phosphate is formed after calcination at 900 °C (c and d). The highly regular, open structure of flame-made calcium phosphate results from sintering the low-density aerosol. Interconnecting pores facilitate liquid circulation through the samples.

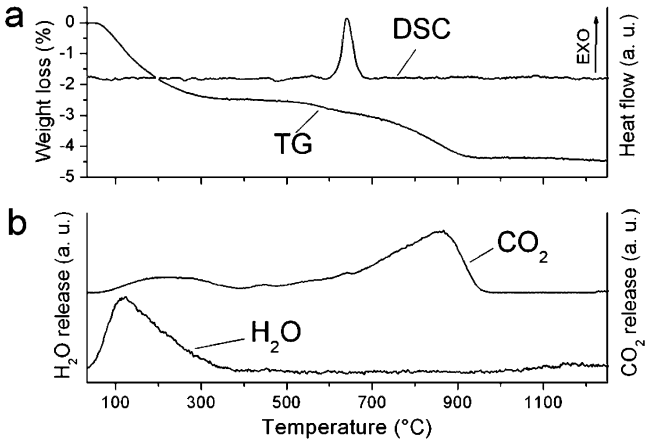

Figure 4. Crystallization and carbon dioxide release properties of Ca/P = 1.67 (apatite stoichiometry). (a) Differential scanning calorimetry (DSC) reveals a clear exothermic peak around 600 °C showing the crystallization of the sample to hydroxyapatite. The weight loss (thermogravimetric curve, TG) during heating is attributed to desorbing water and carbon dioxide from carbonated hydroxyapatite. (b) Water and CO_2 traces as detected by mass spectrometry.

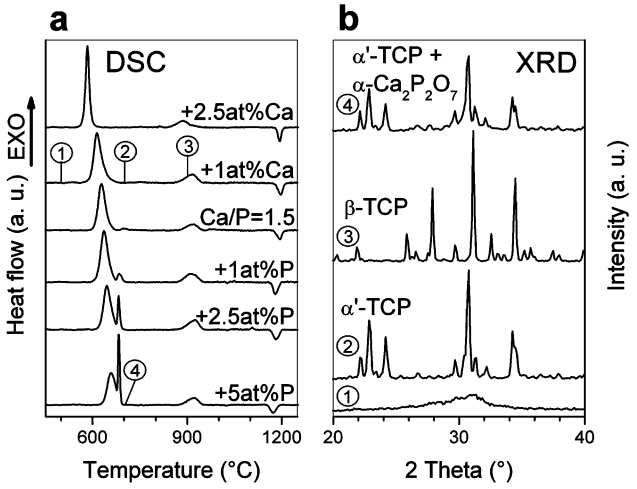

Figure 5. (a) Differential scanning calorimetric measurements of calcium phosphates with decreasing Ca/P ratio. (b) X-ray diffraction pattern of selected samples after a thermal treatment. Samples are amorphous after preparation (trace 1), crystallize to α′-tricalcium phosphate (trace 2) around 600 °C, and undergo a phase transformation to *β*-tricalcium phosphate (trace 3) around 900 °C. Excess phosphorus results in the formation of pyrophosphate (trace 4) with the appearance of two distinct crystallization events between 600 and 700 °C.

pyrophosphate results in a second peak around 690 °C, slightly above the crystallization of tricalcium phosphate (Figure 5, trace 4). A very small pyrophosphate crystallization peak indicates minute amounts of pyrophosphate are present in the stoichiometric sample (Ca/P = 1.5), but they fully vanish with a slight calcium excess (Ca/P = 1.52). Therefore, both pure and calcium phosphate mixtures are accessible by flame synthesis. The sample Ca/P = 1.67 crystallizes to hydroxyapatite above 600 °C (Figure 4a) and no further phase transformation or decomposition could be detected up to 1250 °C.

For all samples, a change in mass attributed to absorbed water on the high-surface materials was detected by thermogravimetry (TG) below 500 °C. Unlike calcium phosphates prepared by wet-phase chemistry, the weight loss of flame-made ceramics did not exceed 3%. A second weight loss (2%) present in the sample with apatite stoichiometry (Ca/P = 1.67) between 500 and 950 °C correlates to the release of CO_2 (Figure 4b). It was previously attributed to the decomposition of carbonate-containing apatite.[31] The presence of carbonate is further evidenced by Fourier transform infrared (FTIR) spectroscopy[32] (Figure 6a) and results in absorption peaks between 1490 and 1420 cm^{-1}

(31) Peters, F.; Schwarz, K.; Epple, M. *Thermochim. Acta* **2000**, *361*, 131−138.
(32) Emerson, W. H.; Fischer, E. E. *Arch. Oral Biol.* **1962**, *7*, 671−683.

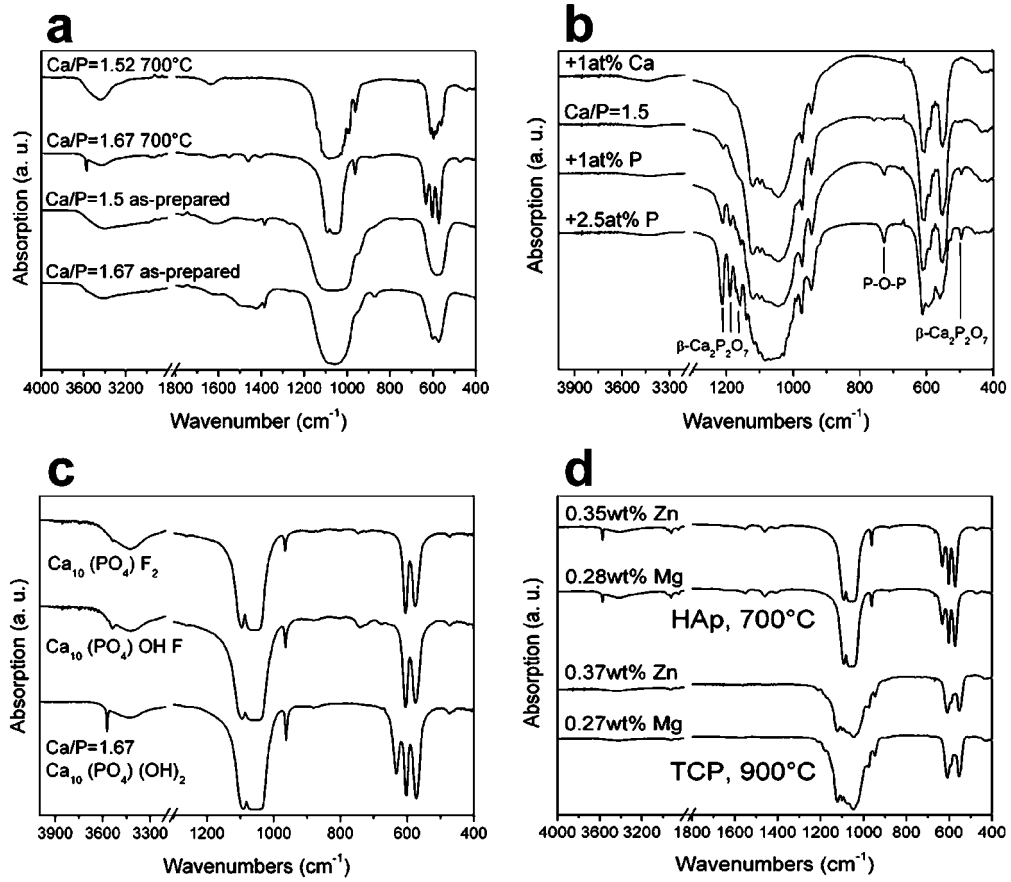

Figure 6. (a) Fourier transform infrared spectra of as-prepared amorphous calcium phosphates (Ca/P = 1.67 and Ca/P = 1.5) results in broad IR bands. After crystallization, the spectra show the typical peak pattern of hydroxyapatite and α′-tricalcium phosphate, respectively. (b) Spectroscopy of different calcium phosphate samples revealed the presence of pyrophosphates as indicated by calorimetry and X-ray diffraction. (c) The spectra of fluorinated hydroxyapatite showed a pattern distinctly different from that of unsubstituted hydroxyapatite. The disappearance of the hydroxyl signal (3572 cm^{-1}) and distinct changes in absorption between 600 and 800 cm^{-1} correlate to the fluoride incorporation. (d) Cation-substituted calcium phosphates show no extra absorption bands of magnesium or zinc compounds. Zn and Mg contents are given as measured by laser ablation inductively coupled plasma mass spectrometry.

and around 870 cm^{-1}. The as-prepared Ca/P = 1.5 sample does not show any of these absorptions. Broad unresolved absorption bands of phosphate around 1060 and 580 cm^{-1} corroborate the amorphous structure of the materials after preparation. Narrow, pronounced absorption peaks were obtained after crystallization corresponding to hydroxyapatite[33] for Ca/P = 1.67 and to α'-TCP[34] for Ca/P = 1.5. Weak water absorption bands are found around 3400 and 1660 cm^{-1} with varying intensity. The crystallized hydroxyapatite still shows minor absorption bands from carbonate[32] between 1550 and 1400 cm^{-1}. From the TG and quantified MS curves (Figure 4) the carbonate content was calculated to be 3.9 wt % CO_3^{2-} which is similar to the content (3−8 wt % CO_3^{2-}) in human bone.[35] The beneficial influence of carbonate in hydroxyapatite has been studied intensively with agreeing conclusions that its incorporation results in higher solubility and enhanced biodegradation.[36,37]

The presence of calcium pyrophosphate, a major impurity in commercial TCP,[38] can be accurately followed by FTIR spectroscopy resulting in absorption peaks at 1215 cm^{-1} to 1140 cm^{-1}, at 727 and 496 cm^{-1} (Figure 6b). Excess phosphorus (Ca/P < 1.5) in tricalcium phosphate is accommodated in the form of β-calcium pyrophosphate (β-$Ca_2P_2O_7$).[39] A continuous decrease of absorption for corresponding peaks follows the decreasing phosphorus content. This gradual decrease of pyrophosphate is further in agreement with thermal analysis measurements (Figure 5). Consequently, the suppression or promotion of calcium pyrophosphate is determined by the Ca/P ratio in the precursor. No calcium pyrophosphate was detected in sample Ca/P = 1.52, where the infrared spectrum matches well with the one of pure β-TCP.[34]

Recent studies about alternative calcium phosphate-based materials have focused on fluoride-substituted hydroxyapatite ($Ca_{10}(PO_4)_6(OH)_{(2-x)}F_x$, where $0 < x < 2$) and fluoro-apatite ($x = 2$). Fluoride, being essential in nutrition, is believed to be required for normal dental and skeletal growth[40] and is thought to increase bone formation by stimulating osteoblast proliferation.[41] The incorporation of fluoride in hydroxyapatite results in enhanced mechanical properties[42] and

(33) Fowler, B. O. *Inorg. Chem.* **1974**, *13*, 194−207.
(34) Jillavenkatesa, A.; Condrate, R. A. *Spectrosc. Lett.* **1998**, *31*, 1619−1634.
(35) Dorozhkin, S. V.; Epple, M. *Angew. Chem. Int. Ed.* **2002**, *41*, 3130−3146.
(36) Fulmer, M. T.; Ison, I. C.; Hankermayer, C. R.; Constantz, B. R.; Ross, J. *Biomaterials* **2002**, *23*, 751−755.
(37) Nelson, D. G. A. *J. Dent. Res.* **1981**, *60*, 1621−1629.
(38) Tadic, D.; Epple, M. *Biomaterials* **2004**, *25*, 987−994.
(39) Hezel, A.; Ross, S. D. *Spectrocim. Acta A* **1967**, *A 23*, 1583.
(40) Mertz, W. *Science* **1981**, *213*, 1332−1338.
(41) Farley, J. R.; Wergedal, J. E.; Baylink, D. J. *Science* **1983**, *222*, 330−332.
(42) Barinov, S. M.; Tumanov, S. V.; Fadeeva, I. V.; Bibikov, V. Y. *Inorg. Mater.* **2003**, *39*, 877−880.

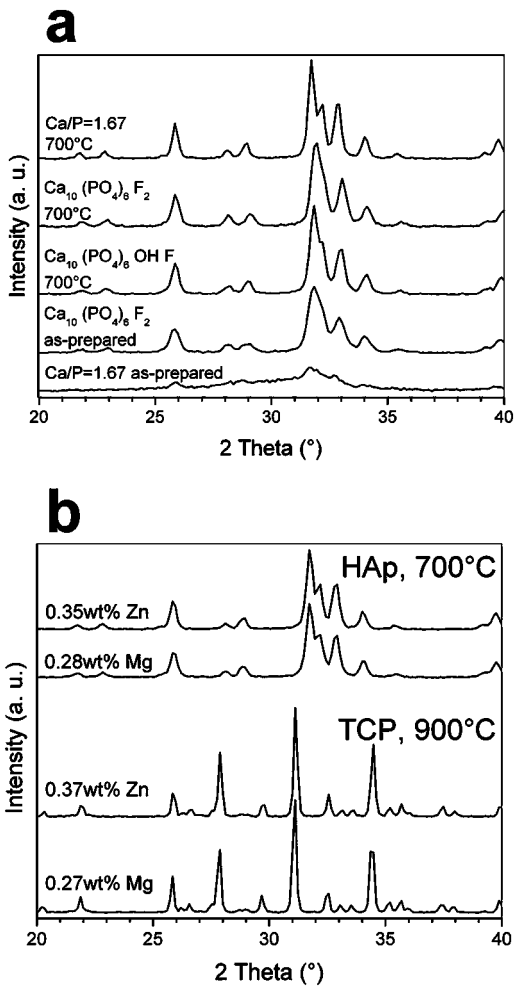

Figure 7. X-ray diffraction pattern of anion- and cation-substituted calcium phosphates. (a) Samples are shown as-prepared (bottom) and after calcination at 700 °C (top). While the unsubstituted apatite (Ca/P = 1.67) only crystallizes after the heat treatment, the as-prepared fluorinated apatite shows a pattern with distinct peaks underlining the crystallinity of the particles as further evidenced by the TEM image. (b) X-ray diffraction patterns of magnesium- and zinc-containing samples showing distinct peaks for TCP and HAp, respectively.

decreased dissolution.[43,44] This effect is used to strengthen teeth and protecting enamel against caries by adding fluoride to toothpaste and mouth rinse. Flame spray synthesis of fluoride-substituted hydroxyapatite (FHAp) resulted in agglomerated, mainly polyhedral-shaped nanoparticles, displaying crystal planes (Figure 2b). The presence of fluoride may afford crystallization despite the fast cooling process in the flame. Both $Ca_{10}(PO_4)_6(OH)F$ and $Ca_{10}(PO_4)_6F_2$ show similar morphology and an increased thermal stability at 700 °C if compared to hydroxyapatite (Figure 2a). While as-prepared Ca/P = 1.67 (apatite stoichiometry) shows a rather amorphous XRD pattern, the fluorine-containing samples display broad but distinct peaks (Figure 7a). After calcination at 700 °C, substituted and pure hydroxyapatite have crystallized. The shift of the peak around 32° for fluoride-substituted samples toward higher 2θ values compared to that of pure Ca/P = 1.67 is attributed to altered lattice parameters as characteristic for FHAp.[45] Together with the absence of additional peaks, this suggests that the fluoride present in the sample is fully incorporated and replaces the lattice hydroxyl.

The comparison of FTIR spectra from sintered HAp (Ca/P = 1.67) and FHAps ($Ca_{10}(PO_4)_6(OH)F$, $Ca_{10}(PO_4)_6F_2$) gives information about the vibrational changes resulting from the incorporation of fluorine (Figure 6c): the broad absorption in the range of 1000 cm^{-1} to 1200 cm^{-1} and the peaks at 962, 602, and 572 cm^{-1}, assigned to the several modes of phosphate (PO_4^{3-}), are obviously not affected by the OH/F substitution. Sample Ca/P = 1.67 shows a sharp O−H stretching band at 3572 cm^{-1}. Substitution of hydroxyl entails a slight shift to lower wavenumbers (3538 cm^{-1} for both FHAps) and a clear reduction in absorption, indicating the ongoing replacement of OH-groups by fluoride. The Ca_3−OH vibrational mode, observed at 632 cm^{-1} in HAp, vanishes and new faint absorption peaks evolve for $Ca_{10}(PO_4)_6(OH)F$ (650, 678, and 740 cm^{-1}) and $Ca_{10}(PO_4)_6F_2$ (648 cm^{-1}). From the detected hydroxyl vibrations and assuming a pure substitution of F for OH, the fluorine content can be estimated[46] to lie between 40 and 50 at. % for $Ca_{10}(PO_4)_6$-(OH)F and above 90 at. % for $Ca_{10}(PO_4)_6F_2$. These results clearly show that complex materials such as fluoro-apatite can be accessible by the one-step flame synthesis.

The cation substitution in tricalcium phosphate and hydroxyapatite has been investigated using physiologically important zinc or magnesium. Zinc-containing calcium phosphates (0.32 wt % Zn) have been reported to stimulate osteogenesis in vivo[47] by slowly releasing zinc ions during the resorption process of the bioceramics. Such materials exhibit the possibility to accelerate post-operative healing and therefore shorten the recovery time of the patient. A constant cation release rate is required to avoid any uncontrolled over-concentration in the vicinity of the implantation site. Therefore, the zinc cation must be homogeneously incorporated in the crystal lattice. The infrared absorption of doped materials (Figure 6d) coincides with the spectrum of TCP or HAp, respectively. The XRD patterns obtained after corresponding calcination confirm the homogeneous incorporation and display no additional phases of zinc- or magnesium-containing compounds (Figure 7b).

Conclusion

The extension of flame spray pyrolysis to complex salt nanoparticles was demonstrated for the preparation of different calcium phosphates. The synthesis of amorphous calcium phosphate with a broad range of compositions and optional doping with additional metals resulted in salt nanoparticles of 10−50-nm size. Phase-pure α- or β-tricalcium phosphate was obtained after calcination of the amorphous particles for a precursor calcium to phosphorus

(43) Moreno, E. C.; Kresak, M.; Zahradnik, R. T. *Nature* **1974**, *247*, 64−65.
(44) Gineste, L.; Gineste, M.; Ranz, X.; Ellefterion, A.; Guilhem, A.; Rouquet, N.; Frayssinet, P. *J. Biomed. Mater. Res.* **1999**, *48*, 224−234.
(45) Wei, M.; Evans, J. H.; Bostrom, T.; Grondahl, L. *J. Mater. Sci.: Mater. Med.* **2003**, *14*, 311−320.
(46) Freund, F.; Knobel, R. M. *J. Chem. Soc., Dalton Trans.* **1977**, 1136−1140.
(47) Kawamura, H.; Ito, A.; Miyakawa, S.; Layrolle, P.; Ojima, K.; Ichinose, N.; Tateishi, T. *J. Biomed. Mater. Res.* **2000**, *50*, 184−190.

molar ratio of 1.52. Excess phosphorus (Ca/P < 1.5) promoted the formation of dicalcium pyrophosphate. Hydroxyapatite is formed from corresponding calcium-rich precursors. As-prepared amorphous apatite (Ca/P = 1.67) contained 3.9 wt % carbonate CO_3^{2-} and crystallizes above 600 °C. Fluoro-apatite nanoparticles resulted from the addition of fluoride to the precursor mixture. After sintering, such materials exhibit a highly regular open structure with interconnecting pores. Facile substitution of anions (F^-) and cations (Mg^{2+} or Zn^{2+}) in calcium phosphate combined with a high degree of flexibility in morphology, crystallinity, and phase composition offer a versatile production tool to biomaterials engineering.

Acknowledgment. This research was financially supported by the Swiss Commission for Technology and Innovation, Top Nano 21, 5978.2, and CTI project 7021.2.

CM048776C